AIP | Applied Physics Letters

Confocal terahertz imaging

N. N. Zinov'ev and A. V. Andrianov

Citation: Appl. Phys. Lett. **95**, 011114 (2009); doi: 10.1063/1.3173200
View online: http://dx.doi.org/10.1063/1.3173200
View Table of Contents: http://apl.aip.org/resource/1/APPLAB/v95/i1
Published by the American Institute of Physics.

Confocal terahertz imaging

N. N. Zinov'ev[a] and A. V. Andrianov
A. F. Ioffe Physical Technical Institute, 194021 St. Petersburg, Russia

(Received 9 March 2009; accepted 17 June 2009; published online 9 July 2009)

We report on a configuration of confocal spatial filtering applied to terahertz imaging. Theoretical analysis of the confocal terahertz imaging layout agrees fairly well with the experimental observations of the enhancement of optical resolving power, both lateral and axial, leading to three-dimensional optical slicing, in comparison with the image properties obtained with a generic terahertz imaging. © *2009 American Institute of Physics*. [DOI: 10.1063/1.3173200]

The current stage of coherent optical imaging operating with terahertz electromagnetic radiation, approached the resolution limit in the focal plane of a far-field terahertz imaging system[1] limited by diffraction. It is scaled down to the mean terahertz wavelength averaged over the irradiated spectrum $\bar{\lambda}_{\mathrm{THz}}$, where $\bar{\lambda}_{\mathrm{THz}} \sim 0.5-1$ mm for a typical terahertz photoconductive antenna or nonlinear crystal emitter. Achieving subwavelength resolution in far-field optics, significant enhancement of imaging contrast and optical slicing can be obtained with the use of spatial filtering[2] and processing both field amplitude and phase variables.[3,4] The earliest and simplest realization of these approaches is known as the confocal microscopy[5–7] and applied to fluorescence imaging in a plethora of biological applications.[8] In this paper we introduce confocal filtering technique to terahertz imaging. It demonstrates significant improvement of the image contrast and resolution overcoming the diffraction limit, which is necessary for a true three-dimensional (3D) optical slicing achieved with terahertz far-field optics.

For the experimental examination of the effect of confocal filtering on terahertz imaging, we used a typical layout of coherent terahertz correlation system[1] modified with the addition of a confocal attachment containing adjustable pinhole filter and focusing condensers. In the equivalent optical scheme [Fig. 1(a)] each effective condenser lens, O_1, O_2, and O_3, corresponded to the pair of parabolic mirrors. Terahertz radiation was generated with a photoconductive antenna, excited by 25 fs pulses of a Ti:sapphire laser ($\lambda = 800$ nm) and average incident power held below 50 mW. The lens O_1 focused terahertz radiation on the subject. The secondary radiation (scattered and transmitted) emanating from the subject, was collected by the condenser lens O_2 and focused into the conjugated focal plane to the subject's one where we placed the pinhole filter. The lens O_3 transformed the image of the pinhole filter onto the input of electro-optic sampling cell. Terahertz detection was accomplished using a free space electro-optic sampling cell[9] equipped with ZnTe crystal of (110) facet orientation and 1 mm thickness. The test phantoms consisted of the bedded stack of Si plates doped with B of resistivity $\rho \simeq 20\ \Omega$ cm and sized at 24×24 mm^2 in plane and thickness of 0.6 mm. A thin layer of Cr of 80 nm thickness was evaporated on the surfaces of each Si plate. The layers of Cr were further lithographically etched into arrays of gratings with different spatial frequencies up to 4 lines/mm, forming the test patterns shown in Fig. 1(b). Each small grating element, mimicking different spatial frequency and coordinated orientations in plane, had the size of 6×6 mm^2, each Si plate had five integrated grating arrays. The separations between Si plates were adjusted to a range of required values with variable spacers. The test phantoms were placed at the center of focal caustic, the focal plane, between the lenses O_1 and O_2. With such alignment we imaged the test phantoms using two-dimensional (2D)-raster scanning of the subject, with reference to the fixed coordinate frame in the objective focal plane. The images were obtained with scanning steps 50 or 100 μm.

If the mean size of terahertz photoconductive antenna $a \ll \bar{\lambda}_{\mathrm{THz}}$, the terahertz emitter can be approximated by a point source. The spread of the focal caustic of the incident terahertz beam is determined by the point spread function (PSF) of O_1, $P_{\mathrm{PSF}}(x,y,z)$, describing the diffraction pattern of electromagnetic wave on the aperture of O_1.[10,11] If a subject is placed in the focal caustic region, then each point of the subject volume enveloped by focusing caustic produces a secondary terahertz radiation due to scattering and absorption mechanisms inside the subject. This secondary terahertz

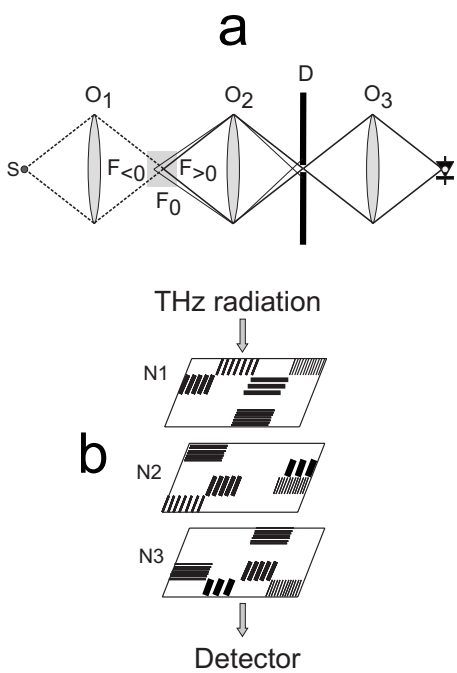

FIG. 1. (a) Equivalent optical scheme for terahertz confocal imaging scheme, where the gray area represents the subject space in the region of focal plane O_1–O_2, and (b) phantom layout.

[a]Electronic mail: nick.zinovev@mail.ioffe.ru.

radiation is determined by the subject's response function S describing the local optical properties, multiplied point by point by the PSF. In fact, S is the function of coordinate differences, $S(x-x_{\text{scan}}, y-y_{\text{scan}}, z-z_{\text{scan}})$ where the variables x_{scan}, y_{scan}, and z_{scan} define a scanner position within the subject's space $\{x,y,z\}$ pierced by terahertz beam [Fig. 1(a)]. The terahertz image of a subject represents the terahertz field pattern $U_{\text{conf}}(x_{\text{scan}}, y_{\text{scan}}, z_{\text{scan}})$ obtained in the confocal scheme of Fig. 1(a) in the coordinate frame of the image space behind the lens O_2 and pinhole as the function of scanner current position x_{scan}, y_{scan}, and z_{scan} is readily derived in the form of

$$U_{\text{conf}}(x_{\text{scan}}, y_{\text{scan}}, z_{\text{scan}}) = \int_V dxdydz S(x-x_{\text{scan}}, y-y_{\text{scan}}, z-z_{\text{scan}}) \times \left\{ P_{\text{PSF}}(x,y,z) \int_{V_d} dx_d dy_d P_{\text{PSF}} \times (x_d - x, y_d - y, z_d - z)|_{z_d=0} \mathcal{D}(x_d, y_d) \right\}, \quad (1)$$

where the term in curly brackets represents the joint confocal PSF, $P_{\text{conf}}(x,y,z)$, that is the product of the PSF of O_1 and the envelope of the PSF of O_2 and pinhole aperture. The effect of confocal pinhole filter is introduced in Eq. (1) via the case function $\mathcal{D}(x_d, y_d)$

$$\mathcal{D}(x_d, y_d) = \begin{cases} 1, & \text{if } \sqrt{x_d^2 + y_d^2} \le r_{\text{pinhole}}, \\ 0, & \text{otherwise}, \end{cases} \quad (2)$$

where r_{pinhole} is the radius of pinhole. The pinhole is placed in the origin of the image coordinate frame. We emphasize, that the direction of coordinate axis X and Y in the image space, is inverted against the coordinate frame of the subject space. For simplicity we assume that the PSFs of all condenser lenses are the same. Noting that all functions in the curly brackets of Eq. (1) obey cylindrical symmetry, we transform it to a more convenient form using optical coordinates defined in Refs. 10 and 11: $u = kz \sin^2 \alpha$ and $v = k\sqrt{x^2+y^2} \sin \alpha = k\rho \sin \alpha$, where α is the angular semiaperture assuming cylindrical symmetry around optical axis and k is the wave vector. Then the joint confocal PSF is transformed to

$$P_{\text{conf}}(v,u) = \mathcal{A} P_{\text{PSF}}(v,u) \times \int_{V_d} v_d dv_d P_{\text{PSF}}(v_d - v, u_d - u)|_{u_d=0} \mathcal{D}(v_d), \quad (3)$$

where $\mathcal{A}$ is the normalization constant. If the diameter of pinhole aperture is much larger than that of the PSF, the envelope integral in Eq. (3) is roughly equal to $\mathcal{D}(v)$ and $P_{\text{conf}}(v,u)$ is proportional to the single lens PSF: $P_{\text{conf}}(v,u) \propto P_{\text{PSF}}(v,u)$. In the opposite limiting case, the diameter of the pinhole is much smaller than the width of PSF central maximum. In this case we approximate $\mathcal{D}(v_d) \to \delta_2(v_d)$, where δ_2 is the 2D delta-function and $P_{\text{conf}}(v,u) \propto P_{\text{PSF}}^2(v,u)$. Taking this limiting case as the top resolution limit for the confocal pinhole radius r_{pinhole} in Eq. (2), $r_{\text{pinhole}} \lesssim v_{\text{Airy}}$, where v_{Airy} is determined by the Airy disk radius, and using the expressions for the structure of the image field obtained in Refs. 10 and 11 for a single lens we find $P_{\text{conf}}(v,u)$ in the focal plane by equating $u=0$

$$P_{\text{conf}_\perp}(v,0) \propto P_{\text{PSF}}^2(v,0) \propto \left(\frac{2\pi a^2}{\lambda f^2}\right)^2 \left[\frac{J_1(v)}{v}\right]^2, \quad (4)$$

while the confocal PSF along the optical axis is expressed by putting $v=0$

$$P_{\text{conf}_\parallel}(0,v) \propto P_{\text{PSF}}^2(0,u) \propto \left(\frac{2\pi a^2}{\lambda f^2}\right)^2 \left[\frac{\sin\left(\frac{u}{2}\right)}{\frac{u}{2}}\right]^2, \quad (5)$$

where a is the radius of lens and f is the focal length. As it follows from Eqs. (4) and (5), the major advantage of adding the confocal filter over the generic scheme for far-field terahertz imaging[1] is not only the enhancement of the axial resolution (5), but also the increase in lateral resolution ability (4). In this case collection of the signal is restricted by a small 3D-pixel, effectively cut off from the interior of a larger subject. The geometry of this 3D-pixel is determined by the forms of transverse and longitudinal confocal PSFs Eqs. (4) and (5), respectively. This allows the examination of small regions within a multiphase system using 3D optical slicing. The pinhole filter strongly suppresses the stray light coming to the receiver from other regions of the subject rather than a chosen 3D-pixel of interest. To obtain a full 3D-image, this 3D-pixel optically sliced off, is moved across the subject in plane and in depth by optical scanners.

To validate the theoretical conclusions outlined above, we measured the spatial resolution in terahertz imaging, both in focal plane and along optical axis. Insertion of the confocal aperture with a chosen diameter, led to the minimal change of the spectral composition of terahertz pulse, but with a reduction in the whole content due to the diaphragm cutoff effect. Figure 2(a) shows terahertz images of one of the phantoms where the focal plane of the pair O_1-O_2 is aligned with the position of the phantom plate N_2 [Fig. 1(b)]. The terahertz signal forming raster image was sampled at the delay time, corresponding to the first major positive half-wave maximum of terahertz electric field waveform. A comparison of terahertz images of the subject in the generic and confocal configurations, shows that the insertion of the confocal aperture yields a considerable enhancement of the contrast and resolution of the subject details. The spatial frequencies of the grating arrays, not resolved in the generic configuration, become perfectly resolved in the confocal scheme of terahertz imaging system. Figure 2(b) depicts the line scans of the terahertz electric field, extracted from the image along the horizontal solid lines, as shown in Fig. 2(a). The line scans in Fig. 2(b) provide the quantitative proofs of the enhancement of both spatial resolution and image contrast achieved with the confocal configuration. It indicates that the ratio of terahertz electric field amplitude minima and maxima in the case of the optical confocal configuration is on average 0.76 for x between $x=3$ mm and $x=7$ mm, which corresponds to the array of metallic strips in plate N_2 with the width and spacing 250 μm [Fig. 1(b)] corresponding to the spatial frequency 4 lines/mm. It is seen that in the case of the generically configured optical system [Fig. 2(b)] curve 1, the same ratio is measured within 0.9–1. Thus, with

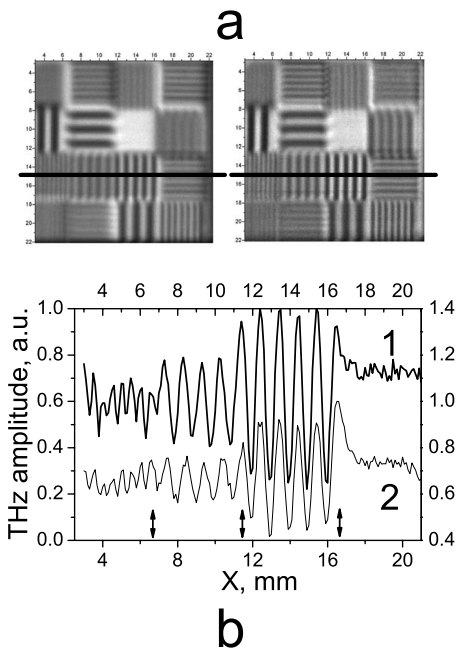

FIG. 2. Demonstration of the enhancement of lateral resolving power: (a) terahertz image of the test phantom with widely open confocal pinhole (left) and with the confocal pinhole of the diameter $2r_{\text{pinhole}}=1.2$ mm (right); (b) terahertz field line scans along the black lines of the images (a), (curve 1) corresponds to the right hand side of (a) and (curve 2) corresponds to the left of (a). The arrows in (b) designate the boarders of grating arrays.

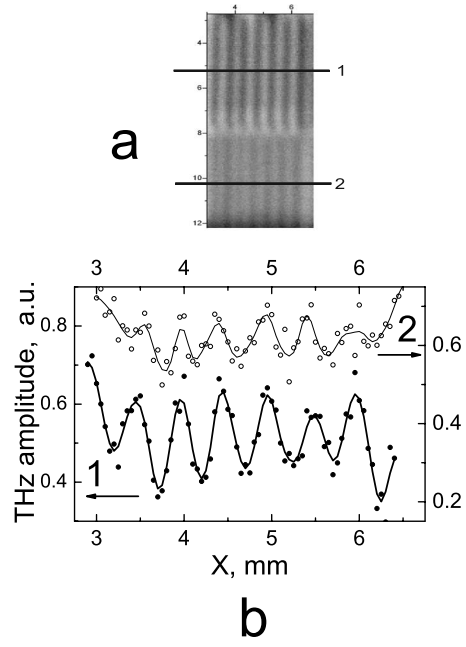

FIG. 3. Demonstration of the enhancement of axial resolving power in the confocal configuration: (a) the upper part of terahertz image is produced by the grating of N_2 (top) placed in the focal plane and the lower part is generated by the identical grating of N_3 offset from the focal plane by $\Delta z \sim \bar{\lambda}_{\text{THz}}$; (b) the line scans of terahertz field along the solid lines 1 and 2, respectively. Solid curves result from smoothing of experimental points.

applied confocal filter the structure with the spatial frequency 4 lines/mm becomes well resolved, according to the Rayleigh criterion.[11] The achieved resolution limits fully agree with the values predicted by Eq. (5).

In order to demonstrate the axial selectivity of confocal terahertz imaging, we performed imaging of two grating arrays with identical major spatial frequencies, N_2 placed in the focal plane and N_3 set in the position with small offset $\Delta z \sim \bar{\lambda}_{\text{THz}}$ along the optical axis. This was achieved by moving the phantom through the focal plane of the objective. Figure 3 demonstrates strong effect on axial object selectivity. In point of fact, the ratio of minimum to maximum of terahertz electric field strength, becomes approximately 0.65 for the phantom N_2 being in the focal plane as is concluded from Fig. 3(b), curve 1. The same parameter takes approximately the value of 0.9 for the phantom N_3 positioned with the offset Δz as follows from Fig. 3(b), curve 2. The experimental data of Fig. 3 indicate that the application of confocal configuration introduces a pronounced improvement of the axial resolution and contrast. If the image contrast is defined as the ratio $\eta=(U_{\max}-U_{\min})/(U_{\max}+U_{\min})$, then the confocal image contrast enhancement in z-direction achieves the increment of 2.5 measured on the phantom array with high spatial frequencies $\gtrsim \bar{\lambda}_{\text{THz}}^{-1}$ that is in agreement with η_{conf}/η calculated from Eq. (5).

To summarize, the experimental studies have demonstrated convincingly the enhancement of both lateral and axial spatial resolution breaking through the diffraction limit, due to the application of confocal optical scheme. It has caused the respective improvement of the image contrast in comparison with the terahertz imaging configuration without application of pinhole filter. The experiments fully back up the theoretical treatment, paving the way toward achieving further increase in subwavelength resolution and optical slicing, using far-field terahertz imaging layout amplified with purpose-designed filtering technique.

We would like to thank J. M. Chamberlain for discussion and A. J. Gallant for processing Si plates for phantoms. We are grateful for financial support to NATO (Grant Nos. CBP.EAP.EV.982445 and CBP.EAV.EV.982445), the Russian Foundation for Basic Research (Grant No. 08-02-00162), and the Federal Agency for Science and Innovations (State Grant No. 02.513.11.3389).

[1]W. L. Chan, J. Deibel, and D. M. Mittleman, Rep. Prog. Phys. **70**, 1325 (2007).
[2]G. Toraldo di Francia, Nuovo Cimento, Suppl. **9**, 426 (1952).
[3]V. A. Andreev and K. V. Indukaev, J. Russ. Laser Res. **24**, 220 (2003).
[4]T. E. Gureyev, T. J. Davis, A. Pogany, S. C. Mayo, and S. W. Wilkins, Appl. Opt. **43**, 2418 (2004).
[5]M. Minsky, Scanning **10**, 128 (1988).
[6]T. Wilson and C. J. R. Sheppard, *Theory and Practice of Scanning Optical Microscopy* (Academic, New York, 1984).
[7]M. Gu, *Principles of Three-Dimensional Imaging in Confocal Microscopes* (World Scientific, Singapore, 1996).
[8]J. B. Pawley, *Handbook of Biological Confocal Microscopy*, 3rd ed. (Springer, New York, 2006).
[9]Q. Wu and X.-C. Zhang, IEEE J. Sel. Top. Quantum Electron. **2**, 693 (1996).
[10]B. Richards and E. Wolf, Proc. R. Soc. London, Ser. A **253**, 358 (1959).
[11]M. Born and E. Wolf, *Principles of Optics* (Pergamon, New York, 1970).